

# Plain strain soil–structure interaction model for a building supported by a circular foundation embedded in a poroelastic half-space

Maria I. Todorovska\*, Yousef Al Rjoub

Department of Civil Engineering, University of Southern California, Los Angeles, CA 90089-2531, USA

Accepted 3 January 2006

## Abstract

A simple theoretical model for soil–structure interaction in water saturated poroelastic soils is presented, developed to explore if the apparent building–foundation–soil system frequency changes due to water saturation. The model consists of a shear wall supported by a rigid circular foundation embedded in a homogenous, isotropic poroelastic half-space, fully saturated by a compressible and inviscid fluid, and excited by in-plane wave motion. The motion in the soil is governed by Biot's theory of wave propagation in fluid saturated porous media. Helmholtz decomposition and wave function expansion of the two P-wave and the S-wave potentials is used to represent the motion in the soil. The boundary conditions along the contact surface between the soil and the foundation are perfect bond (i.e. welded contact) for the skeleton, and either drained or undrained hydraulic condition for the fluid (i.e. pervious or impervious foundation). For the purpose of this exploratory analysis, the zero stress condition at the free surface is relaxed in the derivation of the foundation stiffness matrix, which enables a closed form solution. The implications of this assumption are discussed, based on published comparisons for the elastic case. Also, a closed form representation is derived for the foundation driving forces for incident plane (fast) P-wave or SV wave. Numerical results and comparison with the full-scale measurements are presented in the companion paper, published in this issue.

© 2006 Elsevier Ltd. All rights reserved.

## 1. Introduction

Although most treatments of dynamic soil–structure interaction are based on equivalent single-phase material models of the soil, two-phase models are not uncommon. The two-phase models can be based on the theory of wave propagation in fluid saturated poroelastic soil formulated by Biot [1–4], in which the soil is comprised of a solid skeleton with interconnected pores filled with water. In this model, the motion of the solid is wave motion, governed by the laws of linear elasticity, and the motion of the fluid is diffusion, governed by Darcy's law. Dynamic stiffness and vibrations of rigid *surface* footings on poroelastic half-space or a stratum have been computed and studied by a number of investigators, mostly for vertical motions [5–18]. To the knowledge of the authors, the only such published study for *embedded* foundation is that of Senjuntichai et al.

[19], who consider *vertical* motions only, while there have been no published results for horizontal, rocking and torsional motions of such footings. In this one and in the companion paper [20], we consider *embedded* two-dimensional (2D) foundations, with circular arc cross-section, and show impedances for *horizontal*, *vertical* and *rocking* motion and soil represented by a half-space. Hence, our study, though using a very simple model, adds to the current knowledge of foundation-soil interaction an understanding of the effects of the pore fluid on the *horizontal* and *rocking* impedances of *embedded* foundations. As it will be seen from the results in the companion paper [20], a major difference between impedances for embedded and surface foundations is in the significance of the effect of the pore fluid on the *horizontal* stiffness. While for *surface* footings this effect on the *horizontal* stiffness has been considered less significant (and often omitted from the analysis), our results will show that for *embedded* footings this effect is comparable to the effect on the vertical and rocking stiffness. Biot's original theory [2] and all of the

\*Corresponding author. Tel.: +1 213 740 0616; fax: +1 213 744 1426.  
E-mail address: mtodorov@usc.edu (M.I. Todorovska).

previously mentioned studies are linear, and hence valid for small amplitudes of response. A review of an extension of Biot's theory to *nonlinear* soil response, and applications to soil–structure interaction problems with focus on soil liquefaction can be found in [21]. The following summarizes the findings of the previous studies on rigid surface footings on poroelastic soil.

Halpern and Christiano [5] present compliance matrices for *vertical* and *rocking* motion of a square rigid plate baring on a water saturated poroelastic half-space for water saturated coarse grained sands (with porosity 0.48, and shear modulus of the skeleton 20 times smaller than the bulk modulus of water). Their results indicate smaller (in absolute value) real and imaginary parts of the compliance (i.e. stiffer soil) for saturated soil as compared to dry soils for both vertical and rocking motions. They also studied the stress distribution along the contact surface carried separately by the solid and by the fluid, and concluded that the magnitude of either one of the component stresses can be greater than the total stress predicted by an equivalent undrained elastic solid model (elastic solid with Poisson ratio 0.5).

Philippacopoulos [6] present dynamic stiffness for vertical motion of a rigid disk foundation on a layered poroelastic half-space saturated up to certain depth below the disk. He concludes that “the effect due to saturation on the impedance function is generally not significant. Specifically, at low dimensionless frequency (i.e. less than 3) this effect is practically negligible, while at higher dimensionless frequency (i.e. between 3 and 6), the departure from the dry case was about 30%.” In the discussion of his results, he states “the effect of the pore fluid is to generally reduce the stiffness and increase the damping (compared to the dry case). Furthermore, these effects are more pronounced at higher dimensionless frequency and at lower saturation depth-to-radius ratio. On the other hand, at low frequencies, the results from both saturated and dry cases agree very well.” This was explained by the fact that “the water has sufficient time to drain and thus avoids carrying stresses imposed by the skeleton.” It is not clear from the discussion to what degree the predicted effects are due to the “layer” effect created by the impedance contrast at the water table level at depth, as compared to the fluid motion.

Bougacha et al. [7,8] present a computational model and results for dynamic stiffnesses for rigid strip and circular foundations on fluid filled poroelastic stratum over a rigid base for *horizontal*, *vertical*, *rocking* and *torsional* motion, and propose how to estimate the equivalent properties of an elastic soil. They show results for porosity 0.3, Poisson ratio 1/3, and shear modulus of the skeleton such that it results in shear wave velocity of 152 m/s. For torsional loading, they state that the results for a circular disk obtained for the two-phase medium and the equivalent solid are identical, and explain that by the fact that the torsional loading for circular footings transmits only shear waves into the stratum. They conclude that the seepage

forces introduce substantial damping at low frequencies in the case of vertical excitation, while their effect on the rocking, and especially on the torsional stiffness and damping coefficients were relatively minor.

Kassir and Xu [9] studied interaction of a rigid pervious strip foundation bonded to a poroelastic half-space for *horizontal*, *vertical*, and *rocking* motions. They concluded that the influence of the fluid is substantial, and is more pronounced for vertical and rocking motions. Kassir et al. [10] studied impedances for *vertical* motion of circular footings on a poroelastic half-space. They concluded that, for dense sand, the presence of ground water affects the magnitude and character of the influence functions and should be included in dynamic analysis of surface structures to dynamic loading.

Rajapakse and Senjuntichai [11] present a soil–structure interaction model for rigid strip foundation on a layered half-space, and show results for foundation response to unit vertical and horizontal loads, and vertical impedance for a layered model. They also show results for the pore pressure distribution with depth.

Kassir et al. [12] present impedances for a pervious surface circular footing on a poroelastic half-space, for *rocking* and *horizontal* motions. They conclude that for rocking motion, the presence of pore fluid significantly affects the impedance (both in magnitude and sign), while the influence is marginal for horizontal motion.

Dargush and Chopra [13] consider circular footings on a half-space or a layer over bedrock, for *horizontal*, *vertical*, *rocking* and *torsional* motion. Their results show that for surface footing on half-space, and for vertical motions, the compliance is larger for dry soil than for poroelastic saturated soil, but the difference is small for small frequencies and high permeability. For low permeability, the compliance is similar for poroelastic and for undrained solid. For surface footing on layered medium, they note a significant influence of the soil layer resonances.

Japon et al. [14] show probably the most comprehensive set of results that shed light on the effects of the pore water on the foundation stiffness for surface foundations. They show impedances for strip foundations resting on a half-space, or on a stratum over rigid or compliant bedrock, for smooth or welded contact, and for *horizontal*, *vertical*, and *rocking* motions. Their results show that the seepage forces stiffen the foundation and increase the damping. For a half-space soil model, their results show that the type of contact condition is only important for the real part of *vertical* stiffness, which is larger for a welded contact and for an impervious foundation. Further, the seepage forces produce an effect of increased stiffness for the whole range of frequencies, and their effect is more pronounced on the imaginary part (i.e. the radiation damping). The added density (from the coupling mass term) produces increase in stiffness, noticeable only when there are no seepage forces. For soil represented as a layer, the *vertical* and *rocking* stiffnesses tend to the half-space values as the layer depth grows. At smaller frequencies, the foundation stiffness for

a layer is larger than that for a half-space, but the difference is small for depth of layer to half width of foundation  $>4$ . Further, the foundation stiffness for a layer is oscillatory about the half-space solution, with increasing frequency and decreasing amplitudes of the oscillations as the depth of layer increases. For vertical motions, the oscillations are related to resonance of the fast P-waves in the layer, while for horizontal motions—to the resonance of the SH waves in the layer. Further, they show that the effect of the seepage forces is much more important for a stratum than for half-space, and finally, that the position of the resonant peaks may change substantially with the dissipation coefficient  $b$ .

Zeng and Rajapakse [15] studied *vertical* vibrations of a circular disk on a half-space, and noted an increase in stiffness and radiation damping due to the poroelastic effects.

Bo and Hua [16] present compliances for a circular rigid disk on a half-space for *vertical* motions. They conclude that the difference in compliance between pervious and impervious foundation decreases with increasing seepage forces. Similarly, Jin and Liu [17,18] show such compliances for *horizontal* and for *rocking* motions. For the *horizontal* motions, they conclude that the permeability of the medium has an important effect on horizontal vibrations, and that there is a difference between the compliances for elastic and for saturated half-space. The conclusion for the *rocking* motions is that the difference in compliance between poroelastic and elastic half-space is  $<18\%$  and can be neglected. However, these three studies show results for a very limited set of parameters.

Finally, Senjuntichai et al. [19] show impedances for axisymmetric *embedded* foundations in a half-space for *vertical* motions. They study the effects of foundation depth, soil permeability, and foundation shape. Their results show that for cylindrical shape, both the stiffness and the damping increase with increasing foundation depth. Further, there is a notable dependence of the foundation stiffness on the hydraulic boundary condition especially at higher frequencies and for short cylinders, but this effect is much smaller for smaller permeability.

The model presented in this paper also considers the effects of a structure, in particular a building modeled in 2D as a shear wall, supported by the circular foundation embedded in a poroelastic half-space. Such a soil–structure interaction model has been considered first for semi-circular foundation embedded in an elastic half-space and vertically incident SH waves by Luco [22]. This model was later generalized to obliquely incident SH waves by Trifunac [23] to semi-elliptical foundations by Wong and Trifunac [24], and to P, SV and Rayleigh wave excitation by Todorovska [25,26].

The development of the simple model presented in this paper was motivated by observed correlation of the apparent frequency of a building with rainfall, reported by Clinton et al. [27] for Millikan Library in Pasadena, California. This is a 9-story reinforced concrete structure,

which has been continuously monitored since February of 2001 by a 24 bit tri-axial accelerometer installed on the 9th floor. Data on rainfall is available from the JPL weather station, located about 8.5 km north of the building, for a period of about 2.5 years following installation. The reported changes with heavy rainfall (above 40 mm day) increased in the first and second apparent frequencies of up to about 3% for the EW motions, and recovered in about a week following the rain. The objective of this one and of the companion paper [20] is to explore whether the observed effects might be explained by changes in the foundation soil stiffness due to water saturation. This paper presents the theoretical model. The companion paper [20] shows numerical results for vertically incident SV waves, and a comparison with the full-scale observation at Millikan Library.

## 2. Methodology

### 2.1. The model

The simple two-dimensional soil–structure interaction model is shown in Fig. 1. The structure is represented by a shear beam supported by a circular rigid foundation, with center of curvature at  $O_1$  (Fig. 2), embedded in a homogeneous and isotropic *poroelastic* half-space. The shear beam has height  $H$ , width  $W$ , and mass per unit length  $m_b$ . The foundation has width  $2a$ , depth  $h$ , and mass per unit length  $m_{\text{fnd}}$ . The response of the foundation is described by the horizontal and vertical displacements of point  $O$ ,  $\Delta$  and  $V$ , and the rotation angle  $\varphi$  (positive clockwise). The building moves as a rigid body, with translations  $\Delta$  and  $V$ , and rotation  $\varphi$ , and also deflects due to elastic deformation (Fig. 1). The horizontal displacement at the top of the building due to its relative deformation is  $u_b^{\text{el}}$ . The shear wave velocity in the building is  $V_{S,b}$ , which implies first mode fixed-base frequency  $f_1 = V_{S,b}/(4H)$ . The damping in the building is ignored.

The motion in the half-space is described by the linearized theory of wave propagation in fluid saturated poroelastic media as described by Biot [2]. The two-phase medium is composed of a solid skeleton and fluid occupying completely all of the voids in the skeleton. The properties of this mixture are defined by the shear modulus and Poisson's ratio of the skeleton  $\mu_s$  and  $\nu_s$ , the bulk modulus of the fluid  $K_f$ , the porosity  $\hat{n}$ , the mass density of the grains  $\rho_{\text{gr}}$  comprising the skeleton, and the density of the fluid  $\rho_f$ , both defined per unit volume of pure grain material and pure fluid. This implies shear wave velocity of the dry mixture  $V_{S,\text{dry}} = \sqrt{\mu_s/[(1-\hat{n})\rho_{\text{gr}}]}$ . The skeleton and the foundation are perfectly bonded to each other. The motion of the fluid along the contact surface is constrained, in addition to the motion of the skeleton, by the drainage condition. In this respect, in this paper, the foundation can be either perfectly permeable, allowing for free drainage of the pore fluid, or impermeable. These conditions would

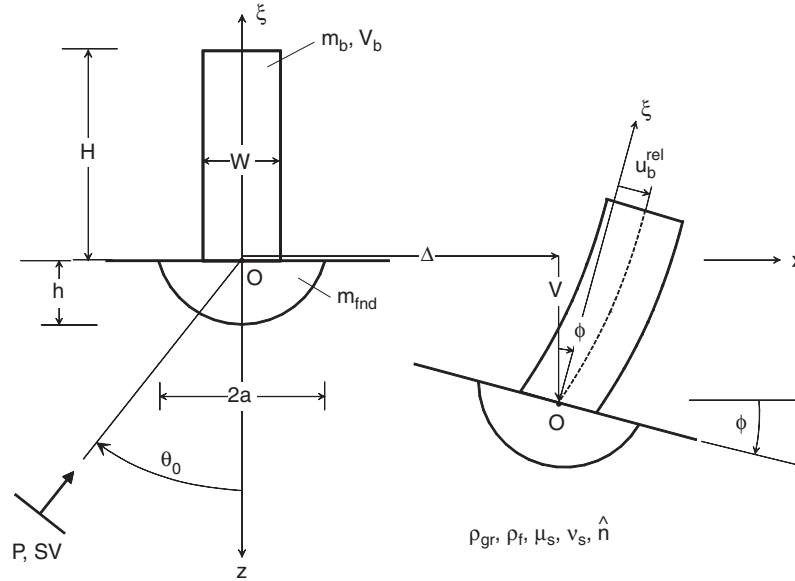


Fig. 1. The model.

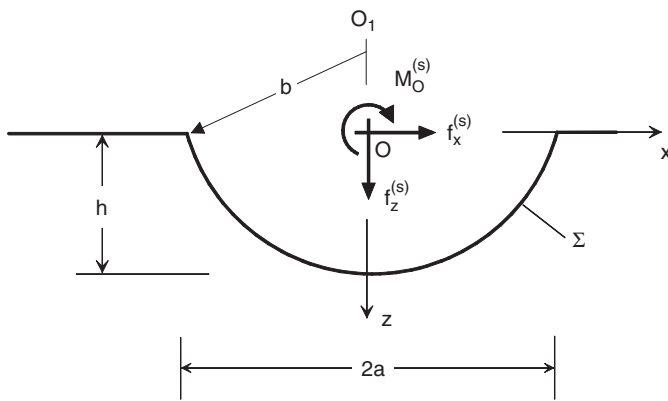


Fig. 2. The excavation and forces acting on the soil.

affect the foundation complex stiffness matrix, and the foundation driving forces. The half-space surface can also be either perfectly sealed or unsealed, and this would affect the free-field motion [28,29].

A closed form solution is obtained by: (1) expanding the scattered waves (a perturbation to the free-field motion caused by the presence of the foundation) in a series of outgoing cylindrical waves (represented by Hankel functions in space); (2) expressing the coefficients of this expansion in terms of the (known) coefficients of expansion of the free-field motion and the (unknown) motion of the rigid foundation through the continuity of displacements at the contact surface; and (3) solving for the motion of the foundation from the dynamic equilibrium conditions. In this process, the zero-stress condition on the half-space surface, which is automatically satisfied by the free-field motion, is relaxed for the scattered waves, assuming that its effect on the final result and conclusions of this study is not very significant.

The decision to relax the zero-stress condition for the scattered waves followed an attempt to derive a closed form solution in which this condition is imposed on the surface of a cylinder with a very large radius and center above the half-space surface, tangent to the half-space in the neighborhood of the structure, and adding an additional field to the scattered waves (represented by Bessel  $J$  functions in space), which is just sufficient to “exactly” solve the problem (see [30] for an application to a problem of wave scattering from an underground cavity). Such a cylindrical surface would start to deviate from the flat half-space only far from the structure, where the amplitudes of the scattered waves are small. However, while such an approximation can be made as good as desired by increasing the radius, and for such a configuration (convex approximation) there is a nontrivial solution of the problem, its implementation revealed that it results in foundation impedance matrix that is *always real*. Physically this means that the model would *not* account for any radiation damping, and, hence, this approximation was abandoned. A proof of this will be presented in a separate publication. Another possibility considered was to approximate the half-space by a concave cylindrical surface (with center below the half-space surface, as in [31], in scattering of P waves from a canyon), which was used by Todorovska [25] in the same problem considered in this paper, but for elastic soil. Besides the conceptual problems of this approximation (only the trivial solution satisfies the boundary condition on the cylindrical half-space approximation), the result of this approximation for large radius are very similar to those corresponding to relaxed zero stress condition for the scattered waves, as shown by de Barros and Luco [32].

The zero stress condition for the scattered waves can be imposed numerically along finite length of the half-space

surface adjacent to the foundation, by some point collocation or a weighted residual method, for example. In the interest of simplicity, and in view of all the other simplifications in this model (e.g., the restriction of the shape of the foundation, the assumption that it is absolutely rigid, the assumption of perfect bond at the contact surface, and finally—the assumption of linear constitutive relations and small displacements, and of homogeneous and isotropic soil), we decided to relax this condition. De Barros and Luco [32] compared foundation impedances for a semi-circular foundation in an elastic half-space, when the zero-stress boundary condition is imposed on the scattered waves, and when it is relaxed. Their results show that for horizontal and vertical motions the difference is small (the approximate solution overestimates slightly the damping and the vertical stiffness, while it underestimated slightly the horizontal stiffness at smaller frequencies and overestimates it slightly for higher frequencies). The difference is also small for the coupling terms (between horizontal motion and rocking). The difference is the largest for the rocking motions at low frequencies, especially for the damping coefficient. The approximate solution overestimates the rocking stiffness and underestimates the damping at all frequencies in the range  $a_0 = \omega a / V_S < 5$ , but the difference becomes progressively smaller as the frequency increases. At  $a_0 = 0.5$ , the rocking stiffness is overestimated by as much as about 28%, and the damping coefficient is underestimated by as much as 38%, but the shapes of the functions are similar, and the difference rapidly decreases with frequency, especially for the damping coefficient. However, it turns out that the rocking stiffness is not noticeably affected by the fluid in the pores, as shown in the companion paper, and therefore the conclusions of this study are not likely to be affected by this approximation.

## 2.2. Biot's theory for wave propagation in porous media

### 2.2.1. Equations of motion

The motion in the half-space is governed by Biot's [2] theory of wave propagation in a fully saturated porous medium, which consists of a skeleton made of solid material and of fluid filling up the voids (pores). This theory is valid for small deformations, laminar flow of the fluid in the pores relative to the solid skeleton (Reynolds number  $< 2000$ ), wavelengths much longer than the size of unit cube, and unit cube much larger than the size of the pores. In the remaining part of this section, this theory is briefly reviewed, following closely the notation used in [33,29].

Let  $\mathbf{u}$  be the displacement vector of the solid-skeleton, and  $\mathbf{U}$  be that of the pore fluid. These displacements satisfy the following equations of motion:

$$\begin{aligned} \mu \nabla^2 \mathbf{u} + \text{grad}[(\lambda + \mu)e + Q\varepsilon] \\ = \frac{\partial^2}{\partial t^2} (\rho_{11} \mathbf{u} + \rho_{12} \mathbf{U}) + \hat{b} \frac{\partial}{\partial t} (\mathbf{u} - \mathbf{U}), \end{aligned} \quad (1)$$

$$\text{grad}[Qe + R\varepsilon] = \frac{\partial^2}{\partial t^2} (\rho_{11} \mathbf{u} + \rho_{12} \mathbf{U}) - \hat{b} \frac{\partial}{\partial t} (\mathbf{u} - \mathbf{U}),$$

where

$$\begin{aligned} e &= \text{div}(\mathbf{u}), \\ \varepsilon &= \text{div}(\mathbf{U}), \end{aligned} \quad (2)$$

$\lambda$  and  $\mu$  are the Lamé moduli of the mixture, and  $Q$  and  $R$  are additional moduli describing the coupling between the two phases. Modulus  $Q$  is a measure of the coupling between the volume change of the solid and that of the fluid, and  $R$  is a measure of the pressure that must be exerted on the fluid to force a given volume of fluid into the mixture with the total volume remaining the same. Further,  $\rho_{11}, \rho_{12}, \rho_{22}$  are dynamic mass coefficients, and  $\hat{b}$  is dissipative coefficient, such that  $\hat{b} = \hat{n}^2 \hat{\mu} / \hat{k}$ , where  $\hat{n}$  is the porosity,  $\hat{k}$  is the permeability coefficient of the fluid, and  $\hat{\mu}$  is the absolute viscosity.

The constitutive relationships for the unit cube of the mixture are:

$$\begin{aligned} \tau_{ij} &= (\lambda e + Q\varepsilon) \delta_{ij} + 2\mu \varepsilon_{ij}, \\ s &= Qe + R\varepsilon, \\ \sigma_{ij}^{\text{tot}} &= \tau_{ij} + s \delta_{ij}, \end{aligned} \quad (3)$$

where  $\tau_{ij}$  is the stress tensor acting on the skeleton,  $s$  is the normal stress acting on the fluid,  $\sigma_{ij}^{\text{tot}}$  is the total stress tensor (all per unit area of the mixture),  $\varepsilon_{ij}$  is the strain tensor for the skeleton, and  $\delta_{ij}$  is the Kronecker delta. The normal stress  $s$  is related to the pore pressure  $p$  (positive when in compression, and per unit area of the fluid inside the pores) by

$$s = -p\hat{n}. \quad (4)$$

A solution of Eqs. (1) can be sought by decomposing the motion into pure dilatation and pure rotation by introducing scalar and vector potentials as follows:

$$\begin{aligned} \mathbf{u} &= \text{grad } \phi + \text{curl } \boldsymbol{\psi}, \\ \mathbf{U} &= \text{grad } \Phi + \text{curl } \boldsymbol{\Psi}, \end{aligned} \quad (5)$$

where  $\phi$  and  $\boldsymbol{\psi}$  are the P- and S-wave potentials for the motion of the solid component, and  $\Phi$  and  $\boldsymbol{\Psi}$  are the corresponding potentials for the motion of the fluid component. The implementation of such decomposition for in-plane motion leads to a harmonic solution of the equations of motion, which is a triplet of two P-waves (one referred to as “regular” or “fast” and the other one as “slow”) and one (vector) S-wave. The additional (slow) P-wave results from the relative motion of the fluid with respect to the solid matrix.

The velocities of the fast and slow P-waves,  $V_{P1}$  and  $V_{P2}$ , and of the S wave,  $V_S$ , are

$$\begin{aligned} V_{Pj} &= \sqrt{\frac{2A}{B \mp (B^2 - 4AC)^{1/2}}}, \quad j = 1, 2, \\ V_S &= \sqrt{\frac{\mu \rho_{22}}{C}}, \end{aligned} \quad (6)$$

where

$$\begin{aligned} A &= PR - Q^2, \\ B &= \rho_{11}R + \rho_{22}P - 2\rho_{12}Q, \\ C &= \rho_{11}\rho_{22} - \rho_{12}^2, \\ P &= \lambda + 2\mu. \end{aligned} \tag{7}$$

For the fast P-wave, the fluid moves in phase with the skeleton, while for the slow P-wave, it moves with opposite phase [2].

Let  $\phi_1$  and  $\phi_2$  be the potentials of the fast and slow P-waves for the motion of the skeleton, and  $\Phi_1$  and  $\Phi_2$  be the same potentials for the motion of the pore fluid. The total  $P$  potentials for the skeleton and for the pore fluid, respectively, are

$$\phi = \phi_1 + \phi_2, \tag{8a}$$

$$\Phi = \Phi_1 + \Phi_2. \tag{8b}$$

The potentials of the fluid motion are related to those of the motion of the skeleton by

$$\Phi_j = f_j \phi_j, \quad j = 1, 2, \tag{9a}$$

$$\Psi = f_3 \psi, \tag{9b}$$

where

$$\begin{aligned} f_j &= \frac{(A/V_{pj}^2) - \rho_{11}R + \rho_{12}Q}{\rho_{12}R - \rho_{22}Q}, \quad j = 1, 2, \\ f_3 &= -\frac{\rho_{12}}{\rho_{22}}. \end{aligned} \tag{10}$$

Hence, the potentials of the fluid do need to be considered explicitly.

### 2.2.2. Material constants for the mixture

The material constants of mixtures can be determined experimentally [34], or can be derived from the properties of the components. In our dimensionless analysis, the input parameters consist of the porosity  $\hat{n}$ , the Poisson's ratio of the skeleton  $\nu_s$ , the ratio of the bulk modulus of the fluid and the shear modulus of the skeleton  $K_f/\mu_s$ , and the ratio of the mass density of the fluid and that of the grains  $\rho_f/\rho_{gr}$  (both per unit volume of "pure" material).

We compute the elastic moduli of the mixture,  $\mu$ ,  $\lambda$ ,  $R$  and  $Q$ , using a simplification (for  $R$  and  $Q$ ) of the formulae proposed by Biot and Willis [34] based on the assumption that the compressibility of the mixture is much smaller than that of the solid skeleton and of the fluid, and can be neglected, which is a common assumption in soil mechanics [29]

$$\begin{aligned} \mu &= \mu_s, \\ \lambda &= \lambda_s + Q^2/R, \\ Q &= (1 - \hat{n})K_f, \\ R &= \hat{n}K_f, \end{aligned} \tag{11}$$

where

$$\lambda_s = 2\nu_s/(1 - 2\nu_s)\mu_s = \text{Lamé constant for the skeleton.}$$

For computing the mass coefficients,  $\rho_{11}$ ,  $\rho_{22}$  and  $\rho_{12}$ , we use the relations proposed by Berryman [35] (also used by Lin et al. [29])

$$\begin{aligned} \rho_{11} &= (1 - \hat{n})\rho_{gr} - \rho_{12}, \\ \rho_{22} &= \hat{n}\rho_f - \rho_{12}, \\ \rho_{12} &= -\hat{n}(\tau_\alpha - 1)\rho_f, \end{aligned} \tag{12}$$

where

$$\tau_\alpha = 1 + \tau_r \frac{1 - \hat{n}}{\hat{n}} \geq 1 \tag{13a}$$

is the dynamic tortuosity. Tortuosity is a dimensionless macroscopic parameter characterizing the resistance to flow of a fluid in porous medium, in particular the effect that, on microscopic scale, the paths of the fluid particles deviate from a straight line. It depends on the porosity,  $\hat{n}$ , as well as on the shape of the pores, through the parameter  $\tau_r$ . It has values  $1 \leq \tau_\alpha < \infty$ . As  $\hat{n} \rightarrow 1$  (pure fluid)  $\tau_\alpha \rightarrow 1$ , and as  $\hat{n} \rightarrow 0$  (pure solid)  $\tau_\alpha \rightarrow \infty$ . For pores formed by spherical grains, which we assume in our analysis,  $\tau_r = 1/2$ , and

$$\tau_\alpha = \frac{1}{2} \left( 1 + \frac{1}{\hat{n}} \right). \tag{13b}$$

It can be seen from Eq. (12) that the dynamic mass coefficients represent physically mass densities, per unit volume of the mixture. If the coupling term  $\rho_{12}$  is neglected, then  $\rho_{11}$  and  $\rho_{22}$  represent the mass densities of the solid and fluid phases per unit volume of the mixture.

### 2.3. Wave fields in the half-space

In the case of seismic wave excitation, the motion in the half-space is the sum of the free-field motion and a perturbation commonly referred to as "scattered" wave field. The excitation can also be a driving force acting on the foundation (e.g. in the case of machine foundations or forced vibrations of buildings).

#### 2.3.1. The free-field motion

The free-field motion is the motion of the half-space without any structure, foundation, or an excavation. We consider free-field motion resulting from the incidence of a plane fast P-wave, and a plane SV wave. Because the slow P-wave attenuates rapidly with distance, only locally generated slow P-waves (by reflections from the free surface and the foundation) are considered, and no such incident waves. These free-field motions have been analyzed in detail by Lin et al. [29], and are only briefly outlined here. In each case, the free-field wave field is described by a triplet of a P-fast, P-slow and S-wave potentials. Because the potentials for the fluid motion can be computed directly from those for the skeleton motion (using Eqs. (9)), only the potentials for the skeleton motion will be considered explicitly, as given quantities, or as unknowns.

Let  $\phi_1^{ff}$  and  $\phi_2^{ff}$  be the total potentials of the free-field fast and slow P-waves, and  $\psi^{ff}$ —that of the SV waves, all for the motion of the skeleton. For an incident plane fast P-wave, the reflection from the free-surface generates three reflected plane waves: fast and slow P-waves, and an SV wave. A similar triplet of reflected waves is generated for an incident plane SV wave below the critical angles. For incidence beyond critical angle, the reflected fast and slow P-waves are surface waves, which have real horizontal phase velocity, but an imaginary vertical phase velocity. The total potentials are sums of the corresponding potentials for the incident and reflected waves. A general representation for the total potentials is

$$\begin{aligned} \phi_1^{ff} &= a_{P1}^i \exp[ik_{P1}(x \sin \theta_{P1}^i - z \cos \theta_{P1}^i) - i\omega t] \\ &\quad + a_{P1}^r \exp[ik_{P1}(x \sin \theta_{P1}^r + z \cos \theta_{P1}^r) - i\omega t], \\ \phi_2^{ff} &= a_{P2}^r \exp[ik_{P2}(x \sin \theta_{P2}^r + z \cos \theta_{P2}^r) - i\omega t], \\ \psi^{ff} &= a_S^i \exp[ik_S(x \sin \theta_S^i - z \cos \theta_S^i) - i\omega t] \\ &\quad + a_S^r \exp[ik_S(x \sin \theta_S^r + z \cos \theta_S^r) - i\omega t], \end{aligned} \tag{14}$$

where  $a_{P1}^i$  and  $a_S^i$  are, respectively, the amplitudes of the potentials for the incident fast P-wave and SV wave,  $a_{P1}^r$ ,  $a_{P2}^r$  and  $a_S^r$  are the amplitudes of the potentials of the reflected fast P, slow P, and SV waves,  $k_{P1}$ ,  $k_{P2}$ , and  $k_S$  are the wave numbers in the medium defined as

$$\begin{aligned} k_{Pj} &\triangleq \omega / V_{Pj}, \quad j = 1, 2, \\ k_S &\triangleq \omega / V_S, \end{aligned} \tag{15}$$

where  $\omega$  is circular frequency,  $\theta_{P1}^i$  and  $\theta_S^i$  are the incident angles of the fast P and of the SV wave, and  $\theta_{P1}^r$ ,  $\theta_{P2}^r$  and  $\theta_S^r$  are the angles of the reflected fast P, slow P and SV waves, all measured from the vertical. The wave velocities in the medium are computed from Eqs. (6), the angles of the reflected waves—from the Snell’s law, and the amplitudes of the reflected waves—from the zero-stress condition. For an unsealed (permeable) half-space boundary, which allows draining of the pore fluid, the zero-stress condition is

$$\left. \begin{matrix} \tau_{zz} \\ \tau_{xz} \\ s \end{matrix} \right\}_{z=0} = \left. \begin{matrix} 0 \\ 0 \\ 0 \end{matrix} \right\} \tag{16a}$$

and for a sealed (impermeable) boundary, which does not allow draining, it is

$$\left. \begin{matrix} \tau_{zz} + s \\ \tau_{xz} \\ U_z - u_z \end{matrix} \right\}_{z=0} = \left. \begin{matrix} 0 \\ 0 \\ 0 \end{matrix} \right\}, \tag{16b}$$

where the stresses are as defined in Eq. (3).

For an incident plane fast P wave, we set  $a_S^i = 0$ , and for unit displacement amplitude incident wave, we set  $a_{P1}^i = 1/k_{P1}$ . The angles of the reflected waves are determined from the Snell’s law

$$\frac{\sin \theta_{P1}^i}{V_{P1}} = \frac{\sin \theta_{P1}^r}{V_{P1}} = \frac{\sin \theta_{P2}^r}{V_{P2}} = \frac{\sin \theta_S^r}{V_S}. \tag{17a}$$

As  $V_{P1} > V_{P2}, V_S$ ,  $\sin \theta_{P2}^r < 1$  and  $\sin \theta_S^r < 1$ , and all of the reflection angles are all always real, i.e. all of the reflected waves are always plane waves.

For an incident plane SV wave, we set  $a_{P1}^i = 0$ , and for unit displacement amplitude incident wave, we set  $a_S^i = 1/k_S$ . The angles of the reflected waves are again determined from the Snell’s law

$$\frac{\sin \theta_S^i}{V_S} = \frac{\sin \theta_{P1}^r}{V_{P1}} = \frac{\sin \theta_{P2}^r}{V_{P2}} = \frac{\sin \theta_S^r}{V_S}, \tag{17b}$$

As  $V_S < V_{P1}$  and possibly  $V_S < V_{P2}$  (depending on the material, and rarely for common soils [29]), the reflected angles for the P waves are not necessarily real. For  $\theta_S^i > \sin^{-1}(V_{P1}/V_S)$ ,  $\sin \theta_{P1}^r > 1$ , and the reflected fast P wave is a surface wave. The same is true for the slow P-wave if  $V_S < V_{P2}$  and  $\theta_S^i > \sin^{-1}(V_{P2}/V_S)$ . Eq. (14) still holds for reflected surface fast and slow P-waves, but with reflection angles that are complex and given by

$$\begin{aligned} \theta_{P1}^r &= \frac{\pi}{2} - i \cosh^{-1} \left( \frac{V_{P1}}{V_S} \sin \theta_S^i \right), \\ \theta_{P2}^r &= \frac{\pi}{2} - i \cosh^{-1} \left( \frac{V_{P2}}{V_S} \sin \theta_S^i \right). \end{aligned} \tag{18}$$

Expressions for the amplitudes of the reflected waves for both sealed and unsealed half-space surfaces can be found in [29], and are not repeated here. Lin et al. [29] also show a detailed analysis of the free-field displacements and point rotations at the surface, as functions of the incident angle, material constants, and surface permeability conditions.

### 2.3.2. The scattered wave field

The scattered waves are represented by a triplet of potentials,  $\phi_1^R$ ,  $\phi_2^R$ , and  $\psi^R$ , each expanded in Fourier–Bessel series with period  $2\pi$ , representing outgoing cylindrical waves with origin along the  $y_1$ -axis (Fig. 2):

$$\begin{aligned} \phi_1^R &= \sum_{n=0}^{\infty} (A_{1,n} \cos n\theta_1 + B_{1,n} \sin n\theta_1) H_n^{(1)}(k_{P1}r_1) e^{-i\omega t}, \\ \phi_2^R &= \sum_{n=0}^{\infty} (E_{1,n} \cos n\theta_1 + F_{1,n} \sin n\theta_1) H_n^{(1)}(k_{P2}r_1) e^{-i\omega t}, \\ \psi^R &= \sum_{n=0}^{\infty} (C_{1,n} \sin n\theta_1 + D_{1,n} \cos n\theta_1) H_n^{(1)}(k_Sr_1) e^{-i\omega t}. \end{aligned} \tag{19}$$

The radial and tangential components of the displacements of the skeleton due to these waves are

$$\begin{aligned} &\left. \begin{matrix} u_{r1} \\ u_{\theta1} \end{matrix} \right\}^R (r_1, \theta_1) \\ &= \left\{ \sum_{n=0}^{\infty} \frac{1}{r_1} \begin{bmatrix} D_{11}^{(3)} \cos n\theta_1 & D_{12}^{(3)} \cos n\theta_1 & D_{13}^{(3)+} \cos n\theta_1 \\ D_{21}^{(3)+} \sin n\theta_1 & D_{22}^{(3)+} \sin n\theta_1 & D_{23}^{(3)} \sin n\theta_1 \end{bmatrix} \right\} \end{aligned}$$

$$\begin{aligned} & \times \begin{Bmatrix} A_{1,n} \\ E_{1,n} \\ C_{1,n} \end{Bmatrix} + \frac{1}{r_1} \begin{bmatrix} D_{11}^{(3)} \sin n\theta_1 & D_{12}^{(3)} \sin n\theta_1 & D_{13}^{(3)-} \sin n\theta_1 \\ D_{21}^{(3)-} \cos n\theta_1 & D_{22}^{(3)-} \cos n\theta_1 & D_{23}^{(3)} \cos n\theta_1 \end{bmatrix} \\ & \times \begin{Bmatrix} B_{1,n} \\ F_{1,n} \\ D_{1,n} \end{Bmatrix} \Bigg\} e^{-i\omega t} \end{aligned} \quad (20a)$$

and the same components of the displacement of the fluid are

$$\begin{aligned} & \begin{Bmatrix} U_{r_1} \\ U_{\theta_1} \end{Bmatrix}^R(r_1, \theta_1) \\ & = \begin{Bmatrix} \sum_{n=0}^{\infty} \frac{1}{r_1} \begin{bmatrix} D_{11}^{(f,3)} \cos n\theta_1 & D_{12}^{(f,3)} \cos n\theta_1 & D_{13}^{(f,3)+} \cos n\theta_1 \\ D_{21}^{(f,3)+} \sin n\theta_1 & D_{22}^{(f,3)+} \sin n\theta_1 & D_{23}^{(f,3)} \sin n\theta_1 \end{bmatrix} \\ & \times \begin{Bmatrix} A_{1,n} \\ E_{1,n} \\ C_{1,n} \end{Bmatrix} + \frac{1}{r_1} \begin{bmatrix} D_{11}^{(f,3)} \sin n\theta_1 & D_{12}^{(f,3)} \sin n\theta_1 & D_{13}^{(f,3)-} \sin n\theta_1 \\ D_{21}^{(f,3)-} \cos n\theta_1 & D_{22}^{(f,3)-} \cos n\theta_1 & D_{23}^{(f,3)} \cos n\theta_1 \end{bmatrix} \\ & + \begin{Bmatrix} B_{1,n} \\ F_{1,n} \\ D_{1,n} \end{Bmatrix} \end{Bmatrix} e^{-i\omega t}. \end{aligned} \quad (20b)$$

The radial and tangential components of the stresses in the skeleton due to these waves are

$$\begin{aligned} & \begin{Bmatrix} \tau_{r_1 r_1} \\ \tau_{r_1 \theta_1} \end{Bmatrix}^R(r_1, \theta_1) \\ & = \frac{2\mu}{r_1^2} \begin{Bmatrix} \sum_{n=0}^{\infty} \begin{bmatrix} E_{11}^{(3)} \cos n\theta_1 & E_{12}^{(3)} \cos n\theta_1 & E_{13}^{(3)+} \cos n\theta_1 \\ E_{21}^{(3)+} \sin n\theta_1 & E_{22}^{(3)+} \sin n\theta_1 & E_{23}^{(3)} \sin n\theta_1 \end{bmatrix} \\ & \times \begin{Bmatrix} A_{1,n} \\ E_{1,n} \\ C_{1,n} \end{Bmatrix} + \begin{bmatrix} E_{11}^{(3)} \sin n\theta_1 & E_{11}^{(3)} \sin n\theta_1 & E_{13}^{(3)-} \sin n\theta_1 \\ E_{21}^{(3)-} \cos n\theta_1 & E_{22}^{(3)-} \cos n\theta_1 & E_{23}^{(3)} \cos n\theta_1 \end{bmatrix} \\ & \times \begin{Bmatrix} B_{1,n} \\ F_{1,n} \\ D_{1,n} \end{Bmatrix} \end{Bmatrix} e^{-i\omega t} \end{aligned} \quad (21a)$$

and the stress in the fluid is

$$\begin{aligned} s^R(r_1, \theta_1) & = \left\{ \sum_{n=0}^{\infty} [E_1^{(f,3)} \cos n\theta_1 \ E_2^{(f,3)} \cos n\theta_1] \begin{Bmatrix} A_{1,n} \\ E_{1,n} \end{Bmatrix} \right. \\ & \left. + [E_1^{(f,3)} \sin n\theta_1 \ E_2^{(f,3)} \sin n\theta_1] \begin{Bmatrix} B_{1,n} \\ F_{1,n} \end{Bmatrix} \right\} e^{-i\omega t}. \end{aligned} \quad (21b)$$

Expressions for  $D_{ij}^{(3)}$ ,  $D_{ij}^{(f,3)}$ ,  $E_{ij}^{(3)}$ , and  $E_{ij}^{(f,3)}$ ,  $i = 1, 2; j = 1, \dots, 3$  are given in Appendix A.

#### 2.4. Boundary conditions at the contact surface

The motion of the rigid foundation for incident monochromatic waves is harmonic, and can be written as

$$\begin{Bmatrix} V \\ \Delta \\ \varphi a \end{Bmatrix} = \begin{Bmatrix} V_0 \\ \Delta_0 \\ \varphi_0 a \end{Bmatrix} e^{-i\omega t}. \quad (22)$$

Along the contact surface  $\Sigma : r_1 = b, -\theta_0 \leq \theta \leq \theta_0$ ,  $\theta_0 = \sin^{-1}(a/b)$  (Fig. 2), the displacements of the skeleton are constrained by the displacements of the foundation, and the motion of the fluid is constrained by the drainage condition. Perfect bond between the skeleton and the foundation, and perfectly sealed contact (i.e. no drainage of the pore fluid) imply

$$\begin{aligned} & \begin{Bmatrix} u_{r_1} \\ u_{\theta_1} \\ (u_{r_1} - U_{r_1})_{\Sigma} \end{Bmatrix}^{\text{ff}} + \begin{Bmatrix} u_{r_1} \\ u_{\theta_1} \\ (u_{r_1} - U_{r_1})_{\Sigma} \end{Bmatrix}^R \\ & = \begin{bmatrix} \cos \theta_1 & \sin \theta_1 & (d/a) \sin \theta_1 \\ -\sin \theta_1 & \cos \theta_1 & -b/a + (d/a) \cos \theta_1 \\ 0 & 0 & 0 \end{bmatrix} \\ & \times \begin{Bmatrix} V_0 \\ \Delta_0 \\ \varphi_0 a \end{Bmatrix} e^{-i\omega t}, \end{aligned} \quad (23a)$$

where the matrix on the right-hand side is the foundation influence matrix. Similarly, perfect bond between the skeleton and the foundation, and unsealed contact (i.e. free drainage of the pore fluid) imply

$$\begin{aligned} & \begin{Bmatrix} u_{r_1} \\ u_{\theta_1} \\ s \end{Bmatrix}_{\Sigma}^{\text{ff}} + \begin{Bmatrix} u_{r_1} \\ u_{\theta_1} \\ s \end{Bmatrix}_{\Sigma}^R \\ & = \begin{bmatrix} \cos \theta_1 & \sin \theta_1 & (d/a) \sin \theta_1 \\ -\sin \theta_1 & \cos \theta_1 & -b/a + (d/a) \cos \theta_1 \\ 0 & 0 & 0 \end{bmatrix} \\ & \times \begin{Bmatrix} V_0 \\ \Delta_0 \\ \varphi_0 a \end{Bmatrix} e^{-i\omega t}. \end{aligned} \quad (23b)$$

The application of these conditions enables expressing the unknown coefficients of expansion of the scattered waves in terms of the known free-field displacements, and the displacements of the foundation. However, this requires expansion of the free-field displacements at  $r_1 = b$  in

Fourier series of  $\theta_1$  with period  $2\pi$ . This can be done by expanding the potentials in Fourier–Bessel series, and then computing the displacements, similarly as for the scattered waves, but such series converge only for the plane waves, and diverge for the surface waves [36]. Hence, for the surface waves, we expand the displacements at  $r_1 = b$  in finite Fourier series of  $\theta_1$ , up to  $n = N$ , which is the truncation index for the expansion of the scattered and plane free-field waves [36]. Let us assume that such expansions are available, with  $A_n^\bullet$  and  $B_n^\bullet$  being the Fourier coefficients for the symmetric and anti-symmetric terms. Then

$$\begin{pmatrix} u_{r_1} \\ u_{\theta_1} \\ (u_{r_1} - U_{r_1}) \end{pmatrix}_\Sigma^{\text{ff}} = \frac{1}{b} \sum_{n=0}^N \left\{ \begin{pmatrix} A_n^{u_r} \cos n\theta_1 \\ A_n^{u_\theta} \sin n\theta_1 \\ (A_n^{u_r} - A_n^{U_r}) \cos n\theta_1 \end{pmatrix} + \begin{pmatrix} B_n^{u_r} \sin n\theta_1 \\ B_n^{u_\theta} \cos n\theta_1 \\ (B_n^{u_r} - B_n^{U_r}) \sin n\theta_1 \end{pmatrix} \right\} \quad (24a)$$

and

$$\begin{pmatrix} u_{r_1} \\ u_{\theta_1} \\ s \end{pmatrix}_\Sigma^{\text{ff}} = \frac{1}{b} \sum_{n=0}^N \left\{ \begin{pmatrix} A_n^{u_r} \cos n\theta_1 \\ A_n^{u_\theta} \sin n\theta_1 \\ A_n^s \cos n\theta_1 \end{pmatrix} + \begin{pmatrix} B_n^{u_r} \sin n\theta_1 \\ B_n^{u_\theta} \cos n\theta_1 \\ B_n^s \sin n\theta_1 \end{pmatrix} \right\}. \quad (24b)$$

For the scattered waves

$$\begin{pmatrix} u_{r_1} \\ u_{\theta_1} \\ (u_{r_1} - U_{r_1}) \end{pmatrix}_\Sigma^R = \frac{1}{b} \sum_{n=0}^N \left\{ \begin{pmatrix} D_{11}^{(3)} \cos n\theta_1 & D_{12}^{(3)} \cos n\theta_1 & D_{13}^{(3)} \cos n\theta_1 \\ D_{21}^{(3)} \sin n\theta_1 & D_{22}^{(3)} \sin n\theta_1 & D_{23}^{(3)} \sin n\theta_1 \\ D_{11}^{(\text{rel},3)} \cos n\theta_1 & D_{12}^{(\text{rel},3)} \cos n\theta_1 & D_{13}^{(\text{rel},3)} \cos n\theta_1 \end{pmatrix}_\Sigma \right. \\ \times \begin{pmatrix} A_{1,n} \\ E_{1,n} \\ C_{1,n} \end{pmatrix} + \begin{pmatrix} D_{11}^{(3)} \cos n\theta_1 & D_{12}^{(3)} \cos n\theta_1 & D_{13}^{(3)} \cos n\theta_1 \\ D_{21}^{(3)} \sin n\theta_1 & D_{22}^{(3)} \sin n\theta_1 & D_{23}^{(3)} \sin n\theta_1 \\ D_{11}^{(\text{rel},3)} \cos n\theta_1 & D_{12}^{(\text{rel},3)} \cos n\theta_1 & D_{13}^{(\text{rel},3)} \cos n\theta_1 \end{pmatrix}_\Sigma \\ \left. \times \begin{pmatrix} B_{1,n} \\ F_{1,n} \\ D_{1,n} \end{pmatrix} \right\}, \quad (25a)$$

where

$$D_{ij}^{(\text{rel},3)} = D_{ij}^{(f,3)} - D_{ij}^{(3)} \quad (25b)$$

and

$$\begin{pmatrix} u_{r_1} \\ u_{\theta_1} \\ s \end{pmatrix}_\Sigma^R = \frac{1}{b} \sum_{n=0}^N \left\{ \begin{pmatrix} D_{11}^{(3)} \cos \theta_1 & D_{12}^{(3)} \cos \theta_1 & D_{13}^{(3)} \cos \theta_1 \\ D_{21}^{(3)} \sin \theta_1 & D_{22}^{(3)} \sin \theta_1 & D_{23}^{(3)} \sin \theta_1 \\ E_{11}^{(f,3)} \cos \theta_1 & E_{12}^{(f,3)} \cos \theta_1 & E_{13}^{(f,3)} \cos \theta_1 \end{pmatrix}_\Sigma \right. \\ \times \begin{pmatrix} A_{1,n} \\ E_{1,n} \\ C_{1,n} \end{pmatrix} + \begin{pmatrix} D_{11}^{(3)} \cos \theta_1 & D_{12}^{(3)} \cos \theta_1 & D_{13}^{(3)} \cos \theta_1 \\ D_{21}^{(3)} \sin \theta_1 & D_{22}^{(3)} \sin \theta_1 & D_{23}^{(3)} \sin \theta_1 \\ E_{11}^{(f,3)} \cos \theta_1 & E_{12}^{(f,3)} \cos \theta_1 & E_{13}^{(f,3)} \cos \theta_1 \end{pmatrix}_\Sigma \\ \left. \times \begin{pmatrix} B_{1,n} \\ F_{1,n} \\ D_{1,n} \end{pmatrix} \right\}. \quad (25c)$$

After substitution for the appropriate expansions in Eqs. (25a) and (25b), and matching the terms multiplying the same basis functions (due to the orthogonality of Fourier series), the coefficients of expansion of the scattered field can be expressed in terms of the coefficients of expansion of the free-field motion and the displacements of the foundation. Then for sealed boundary

$$\begin{pmatrix} A_{1,n} \\ E_{1,n} \\ C_{1,n} \end{pmatrix} = [D_{\Sigma, \text{sealed}}^{(3)+}]^{-1} \left\{ - \begin{pmatrix} A_n^{u_r} \\ A_n^{u_\theta} \\ A_n^{u_r} - A_n^{U_r} \end{pmatrix} + [X^+(n)] \begin{pmatrix} V_0 \\ \Delta_0 \\ \varphi_0 a \end{pmatrix} \right\}, \quad n = 0, \dots, N, \\ \begin{pmatrix} B_{1,n} \\ F_{1,n} \\ D_{1,n} \end{pmatrix} = [D_{\Sigma, \text{sealed}}^{(3)-}]^{-1} \left\{ - \begin{pmatrix} B_n^{u_r} \\ B_n^{u_\theta} \\ B_n^{u_r} - B_n^{U_r} \end{pmatrix} + [X^-(n)] \begin{pmatrix} V_0 \\ \Delta_0 \\ \varphi_0 a \end{pmatrix} \right\}, \quad n = 0, \dots, N, \quad (26a)$$

and for an unsealed boundary

$$\begin{pmatrix} A_{1,n} \\ E_{1,n} \\ C_{1,n} \end{pmatrix} = [D_{\Sigma, \text{unsealed}}^{(3)+}]^{-1} \left\{ - \begin{pmatrix} A_n^{u_r} \\ A_n^{u_\theta} \\ A_n^s \end{pmatrix} + [X^+(n)] \begin{pmatrix} V_0 \\ \Delta_0 \\ \varphi_0 a \end{pmatrix} \right\}, \quad n = 0, \dots, N,$$

$$\begin{Bmatrix} B_{1,n} \\ F_{1,n} \\ D_{1,n} \end{Bmatrix} = [D_{\Sigma,unsealed}^{(3)+}]^{-1} \begin{Bmatrix} B_n^{u_r} \\ B_n^{u_\theta} \\ B_n^s \end{Bmatrix} + [X^-(n)] \begin{Bmatrix} V_0 \\ \Delta_0 \\ \varphi_0 a \end{Bmatrix}, \quad n = 0, \dots, N, \quad (26b)$$

where

$$[D_{\Sigma,sealed}^{(3)\pm}] = \begin{bmatrix} D_{11}^{(3)} & D_{12}^{(3)} & D_{13}^{(3)} \\ D_{21}^{(3)} & D_{22}^{(3)} & D_{23}^{(3)} \\ D_{11}^{(rel,3)} & D_{12}^{(rel,3)} & D_{13}^{(rel,3)} \end{bmatrix}^\pm (n, b),$$

$$[D_{\Sigma,unsealed}^{(3)\pm}] = \begin{bmatrix} D_{11}^{(3)} & D_{12}^{(3)} & D_{13}^{(3)} \\ D_{21}^{(3)} & D_{22}^{(3)} & D_{23}^{(3)} \\ E_{11}^{(f,3)} & E_{12}^{(f,3)} & E_{13}^{(f,3)} \end{bmatrix}^\pm (n, b), \quad (27)$$

and

$$[X^+(n)] = \begin{bmatrix} -1 & 0 & 0 \\ 0 & 0 & 0 \\ 0 & 0 & 0 \end{bmatrix}, \quad n = 1,$$

$$[X^+(n)] = \begin{bmatrix} 0 & 0 & 0 \\ 0 & 0 & 0 \\ 0 & 0 & 0 \end{bmatrix}, \quad n \neq 1, \quad (28a)$$

$$[X^-(n)] = \begin{bmatrix} 0 & 0 & 0 \\ 0 & 0 & -b/a \\ 0 & 0 & 0 \end{bmatrix}, \quad n = 0,$$

$$[X^-(n)] = \begin{bmatrix} 0 & 1 & d/a \\ 0 & 1 & d/a \\ 0 & 0 & 0 \end{bmatrix}, \quad n = 1,$$

$$[X^-(n)] = \begin{bmatrix} 0 & 0 & 0 \\ 0 & 0 & 0 \\ 0 & 0 & 0 \end{bmatrix}, \quad n > 1. \quad (28b)$$

### 2.5. Integral of stresses along the contact surface

Next we compute vertical and horizontal forces  $f_z^{(s)}$  and  $f_x^{(s)}$ , and moment about  $O$ ,  $M_0^{(s)}$ , which result from all stresses in the soil along the contact surface  $\Sigma$ , and have signs as shown in Fig. 2. We also introduce a generalized force vector notation for this triplet of forces and moment  $\mathbf{F} = \{f_z, f_x, M_0/a\}^T$  and refer to it as *the force*, and generalized displacement vector  $\mathbf{\Delta} = \{V, \Delta, \varphi a\}^T$  and refer to it as *the displacement*. For harmonic excitation,  $\mathbf{\Delta}$  is also

harmonic and can be written as

$$\mathbf{\Delta} = \mathbf{\Delta}_0 e^{-i\omega t}, \quad (29)$$

where  $\mathbf{\Delta}_0$  is its complex amplitude.

The resultant force vector,  $\mathbf{F}^{(s)}$ , is the sum of the force vectors due to the free-field motion and due to the scattered waves,  $\mathbf{F}_{ff}^{(s)}$  and  $\mathbf{F}_R^{(s)}$ , and can be computed as follows:

$$\mathbf{F}^{(s)} = \mathbf{F}_{ff}^{(s)} + \mathbf{F}_R^{(s)}$$

$$= \int_{-\theta_0}^{\theta_0} b \begin{bmatrix} -\cos \theta_1 & +\sin \theta_1 \\ -\sin \theta_1 & -\cos \theta_1 \\ -(d/a)\sin \theta_1 & b/a - (d/a)\cos \theta_1 \end{bmatrix} \times \left\{ \left\{ \begin{matrix} \tau_{r_1 r_1} + s \\ \tau_{r_1 \theta_1} \end{matrix} \right\}_{\Sigma}^{ff} + \left\{ \begin{matrix} \tau_{r_1 r_1} + s \\ \tau_{r_1 \theta_1} \end{matrix} \right\}_{\Sigma}^R \right\} d\theta_1. \quad (30)$$

Eq. (30) holds for both sealed and unsealed conditions. We note however that, for an unsealed boundary, the total stress in the pore fluid,  $s^{ff} + s^R$ , is actually zero on the boundary, as preset by the drainage condition (see Eq. (23b)).

Similarly as in Section 2.4, we expand the stresses of the free-field motion along the contact surface in Fourier series of  $\theta_1$  with period  $2\pi$

$$\left\{ \begin{matrix} \tau_{r_1 r_1} + s \\ \tau_{r_1 \theta_1} \end{matrix} \right\}_{\Sigma}^{ff} = \frac{2\mu}{b^2} \sum_{n=0}^N \left\{ \left\{ \begin{matrix} (A_n^{\tau_{rr}} + A_n^s) \cos n\theta_1 \\ A_n^{\tau_{r\theta}} \sin n\theta_1 \end{matrix} \right\} + \left\{ \begin{matrix} (B_n^{\tau_{rr}} + B_n^s) \sin n\theta_1 \\ B_n^{\tau_{r\theta}} \cos n\theta_1 \end{matrix} \right\} \right\} e^{-i\omega t} \quad (31)$$

and substitute in Eq. (30). Then, for the forces due to the free-field motion we get

$$\mathbf{F}_{ff}^{(s)} = \frac{2\mu}{b} \sum_{n=0}^N \left\{ [L^+(n)] \left\{ \begin{matrix} A_n^{\tau_{rr}} + A_n^s \\ A_n^{\tau_{r\theta}} \end{matrix} \right\} + [L^-(n)] \left\{ \begin{matrix} B_n^{\tau_{rr}} + B_n^s \\ B_n^{\tau_{r\theta}} \end{matrix} \right\} \right\} e^{-i\omega t}, \quad (32)$$

where

$$[L^+(n)] = \int_{-\theta_0}^{\theta_0} \begin{bmatrix} -\cos \theta_1 \cos n\theta_1 & \sin \theta_1 \sin n\theta_1 \\ -\sin \theta_1 \cos n\theta_1 & -\cos \theta_1 \sin n\theta_1 \\ -(d/a)\sin \theta_1 \cos n\theta_1 & [b/a - (d/a)\cos \theta_1] \sin n\theta_1 \end{bmatrix} d\theta_1,$$

$$[L^-(n)] = \int_{-\theta_0}^{\theta_0} \begin{bmatrix} -\cos \theta_1 \sin n\theta_1 & \sin \theta_1 \cos n\theta_1 \\ -\sin \theta_1 \sin n\theta_1 & -\cos \theta_1 \cos n\theta_1 \\ -(d/a)\sin \theta_1 \sin n\theta_1 & [b/a - (d/a)\cos \theta_1] \cos n\theta_1 \end{bmatrix} d\theta_1. \quad (33)$$

Some of the terms of matrices  $[L^+(n)]$  and  $[L^-(n)]$  are automatically zero (when the integrand is an odd function), and the nonzero ones can be evaluated

analytically, which gives

$$\begin{aligned}
 [L^+(n)] &= \begin{bmatrix} -I_1(n) & I_4(n) \\ 0 & 0 \\ 0 & 0 \end{bmatrix}, \\
 [L^-(n)] &= \begin{bmatrix} 0 & 0 \\ -I_4(n) & -I_1(n) \\ -(d/a)I_4(n) & (b/a)I_5(n) - (d/a)I_1(n) \end{bmatrix}. \quad (34)
 \end{aligned}$$

The expressions for the integrals  $I_1(n)$ ,  $I_4(n)$ , and  $I_5(n)$  are given in Appendix B. Similarly, for the forces from the scattered waves we get

$$\begin{aligned}
 \mathbf{F}_R^{(s)} &= \frac{2\mu}{b} \sum_{n=0}^N \left\{ [L^+(n)][E_\Sigma^{(3)+}(n)] \begin{Bmatrix} A_{1,n} \\ E_{1,n} \\ C_{1,n} \end{Bmatrix} \right. \\
 &\quad \left. + [L^-(n)][E_\Sigma^{(3)-}(n)] \begin{Bmatrix} B_{1,n} \\ F_{1,n} \\ D_{1,n} \end{Bmatrix} \right\} e^{-i\omega t}, \quad (35)
 \end{aligned}$$

where

$$\begin{aligned}
 [E_\Sigma^{(3)\pm}(n)] &= \begin{bmatrix} E_{11}^{(3)} + E_{11}^{(f,3)} & E_{12}^{(3)} + E_{12}^{(f,3)} & E_{13}^{(3)} + E_{13}^{(f,3)} \\ E_{21}^{(3)} & E_{22}^{(3)} & E_{23}^{(3)} \end{bmatrix}^\pm (n, b). \quad (36)
 \end{aligned}$$

Further, substituting in Eq. (34) for the coefficients of expansion of the scattered waves from Eq. (26a), (26b) it follows that for a sealed boundary

$$\begin{aligned}
 \mathbf{F}_R^{(s)} &= \frac{2\mu}{b} \sum_{n=0}^N \left\{ [L^+(n)][E_\Sigma^{(3)+}(n)][D_{\Sigma,sealed}^{(3)+}]^{-1} \right. \\
 &\quad \times \left\{ - \begin{Bmatrix} A_n^{u_r} \\ A_n^{u_\theta} \\ A_n^{u_r} - A_n^{u_r} \end{Bmatrix} + b[X^+(n)] \begin{Bmatrix} V_0 \\ \Delta_0 \\ \varphi_0 a \end{Bmatrix} \right\} \\
 &\quad \left. + [L^-(n)][E_\Sigma^{(3)-}(n)][D_{\Sigma,sealed}^{(3)-}]^{-1} \right\} \\
 &\quad \times \left\{ - \begin{Bmatrix} B_n^{u_r} \\ B_n^{u_\theta} \\ B_n^{u_r} - B_n^{u_r} \end{Bmatrix} + b[X^-(n)] \begin{Bmatrix} V_0 \\ \Delta_0 \\ \varphi_0 a \end{Bmatrix} \right\} e^{-i\omega t}. \quad (37)
 \end{aligned}$$

It is seen that  $\mathbf{F}_R^{(s)}$  depends both on the displacements from the free-field motion and that of the foundation, and can be written as

$$\mathbf{F}_R^{(s)} = \mathbf{F}_{scat}^{(s)} + \mathbf{F}_A^{(s)}, \quad (38)$$

where

$$\mathbf{F}_A^{(s)} = 2\mu[K^{(s)}]\mathbf{\Delta} \quad (39)$$

with

$$\begin{aligned}
 [K^{(s)}] &= 2\mu \sum_{n=0}^N \left\{ [L^+(n)][E_\Sigma^{(3)+}(n)][D_{\Sigma,sealed}^{(3)+}]^{-1}[X^+(n)] \right. \\
 &\quad \left. + [L^-(n)][E_\Sigma^{(3)-}(n)][D_{\Sigma,sealed}^{(3)-}]^{-1}[X^-(n)] \right\} \quad (40)
 \end{aligned}$$

and

$$\begin{aligned}
 \mathbf{F}_{scat}^{(s)} &= -\frac{2\mu}{b} \sum_{n=0}^N \left\{ [L^+(n)][E_\Sigma^{(3)+}(n)][D_{\Sigma,sealed}^{(3)+}]^{-1} \right. \\
 &\quad \left\{ \begin{Bmatrix} A_n^{u_r} \\ A_n^{u_\theta} \\ A_n^{u_r} - A_n^{u_r} \end{Bmatrix} \right\} + [L^-(n)][E_\Sigma^{(3)-}(n)][D_{\Sigma,sealed}^{(3)-}]^{-1} \\
 &\quad \left\{ \begin{Bmatrix} B_n^{u_r} \\ B_n^{u_\theta} \\ B_n^{u_r} - B_n^{u_r} \end{Bmatrix} \right\} \right\} e^{-i\omega t}. \quad (41)
 \end{aligned}$$

For an unsealed boundary

$$\begin{aligned}
 [K^{(s)}] &= \sum_{n=0}^N \left\{ [L^+(n)][E_\Sigma^{(3)+}(n)][D_{\Sigma,unsealed}^{(3)+}]^{-1}[X^+(n)] \right. \\
 &\quad \left. + [L^-(n)][E_\Sigma^{(3)-}(n)][D_{\Sigma,unsealed}^{(3)-}]^{-1}[X^-(n)] \right\} \quad (42)
 \end{aligned}$$

and

$$\begin{aligned}
 \mathbf{F}_{scat}^{(s)} &= -\frac{2\mu}{b} \sum_{n=0}^N \left\{ [L^+(n)][E_\Sigma^{(3)+}(n)][D_{\Sigma,unsealed}^{(3)+}]^{-1} \right. \\
 &\quad \left\{ \begin{Bmatrix} A_n^{u_r} \\ A_n^{u_\theta} \\ A_n^s \end{Bmatrix} \right\} \\
 &\quad \left. + [L^-(n)][E_\Sigma^{(3)-}(n)][D_{\Sigma,unsealed}^{(3)-}]^{-1} \right\} \left\{ \begin{Bmatrix} B_n^{u_r} \\ B_n^{u_\theta} \\ B_n^s \end{Bmatrix} \right\} e^{-i\omega t}. \quad (43)
 \end{aligned}$$

Then the integral of all stresses in the soil along the contact surface is

$$\begin{aligned}
 \mathbf{F}^{(s)} &= \mathbf{F}_{ff}^{(s)} + \mathbf{F}_{scat}^{(s)} + \mathbf{F}_A^{(s)} \\
 &= \mathbf{F}_{driv}^{(s)} + \mathbf{F}_A^{(s)}, \quad (44)
 \end{aligned}$$

where

$$\mathbf{F}_{driv}^{(s)} = \mathbf{F}_{ff}^{(s)} + \mathbf{F}_{scat}^{(s)}. \quad (45)$$

The interpretation of these forces and of matrix  $[K^{(s)}]$  is as follows.  $\mathbf{F}_A^{(s)}$  defined by Eq. (39) is an external force required to move the foundation by displacement  $\mathbf{\Delta}$  when there is no free-field motion, and the matrix relating them,  $2\mu[K^{(s)}]$ , is the foundation stiffness matrix. This matrix is complex, with its real part representing the stiffness of the foundation, and its imaginary part the radiation damping.  $\mathbf{F}_{driv}^{(s)}$  defined by Eq. (45) is the external force required to

hold the foundation in place when it is subjected to the action of the free-field waves. Its reaction is the force with which the free-field motion *effectively* drives the foundation, and is the generalized *foundation driving force*. It is different from force  $\mathbf{F}_{\text{ff}}^{(s)}$ , which is the integral of the stresses of the free-field motion, because of the scattering of waves from the foundation.

### 2.6. Dynamic equilibrium of the foundation

The only remaining unknown is the foundation displacement vector,  $\Delta$ , which can be determined from the dynamic equilibrium condition for the foundation. Fig. 3 shows a free-body diagram of the foundation, which is subjected to the forces from the building,  $\mathbf{F}^{(b)}$ , and the forces from the soil,  $\mathbf{F}^{(s)} = \mathbf{F}_{\text{driv}}^{(s)} + 2\mu[\mathbf{K}^{(s)}]\Delta$ . For small amplitudes of the response, the forces from the building can be represented in terms of the displacement vector,  $\Delta$ , as follows [26]:

$$\mathbf{F}^{(b)} = m_b \omega^2 [M_b] \Delta, \quad (46)$$

where  $[M_b]$  is a dimensionless matrix that depends on the building model and characteristics. For a shear beam model, and neglecting the effect of the gravity forces, its entries are

$$\begin{aligned} M_{b,11} &= \frac{\tan(\omega H/V_{P,b})}{\omega H/V_{P,b}}, \\ M_{b,22} &= \frac{\tan(\omega H/V_{S,b})}{\omega H/V_{S,b}}, \\ M_{b,23} &= M_{b,32} = \frac{-1}{(\omega H/V_{S,b})^2} (1 - 1/\cos(\omega H/V_{S,b})) \frac{H}{a}, \\ M_{b,33} &= \left[ \frac{1}{(\omega H/V_{S,b})^2} \left( 1 - \frac{\tan(\omega H/V_{S,b})}{\omega H/V_{S,b}} \right) \right. \\ &\quad \left. + \frac{1}{12} (W/H)^2 \right] \left( \frac{H}{a} \right)^2. \end{aligned} \quad (47)$$

In Eqs. (46) and (47),  $m_b$  is the mass per unit length of the beam, and  $H$  and  $W$  are its height and width, and  $V_{S,b}$  and

$V_{P,b}$  are its S and P-wave velocities. The dynamic equilibrium of forces acting onto the foundation implies

$$\omega^2 m_{\text{fnd}} [M_{\text{fnd}}] \Delta - \mathbf{F}_{\text{driv}}^{(s)} - 2\mu[\mathbf{K}^{(s)}] \Delta + \omega^2 m_b [M_b] \Delta = \mathbf{0}, \quad (48)$$

where  $m_{\text{fnd}}$  is the mass of the foundation,  $[M_{\text{fnd}}]$  is the foundation dimensionless mass matrix

$$[M_{\text{fnd}}] = \begin{bmatrix} 1 & 0 & 0 \\ 0 & 1 & 0 \\ 0 & 0 & I_{\text{fnd},0}/(m_{\text{fnd}} a^2) \end{bmatrix}, \quad (49)$$

where

$$\begin{aligned} I_{\text{fnd},0} &= \frac{b^2 m_{\text{fnd}}}{\theta_0 - \sin \theta_0 \cos \theta_0} \\ &\quad \times \left[ \left( \frac{1}{2} + \cos^2 \theta_0 \right) \theta_0 - \frac{3}{2} \sin \theta_0 \cos \theta_0 \right] \end{aligned} \quad (50)$$

is the mass moment of inertia of the foundation relative to point  $O$ , and  $m_{\text{fnd}}$  is the mass per unit length of the foundation. Finally, one can solve for  $\Delta$  by inverting a  $3 \times 3$  matrix

$$\Delta = \left[ \frac{\omega^2 m_{\text{fnd}}}{2\mu} [M_{\text{fnd}}] + \frac{\omega^2 m_b}{2\mu} [M_b] - [\mathbf{K}^{(s)}] \right]^{-1} 2\mu \mathbf{F}_{\text{driv}}^{(s)}. \quad (51)$$

For the purpose of brevity, and without loss of generality, the dynamic moments of the gravity forces were neglected in the above derivations. The expressions including these moments can be found in [25,26].

### 3. Discussion and conclusions

This paper presented a simple 2D model of soil–structure interaction for a building represented as a shear beam, supported by a circular embedded foundation embedded in a homogeneous poroelastic half-space. The solution is based on Biot’s theory of wave propagation in fully saturated soils. The wave-function expansion method was used to represent the motion in the soil, and a closed form solution was obtained for the foundation stiffness matrix and for the system response. The scattered waves were represented by outgoing waves that satisfy the continuity conditions and the hydraulic condition on the contact surface between the soil and the foundation, while the zero-stress condition on the half-space surface was relaxed.

The solution of the problem can be expressed entirely in terms of dimensionless parameters. We defined those using reference: length  $a$ , material modulus  $\mu_s$ , and mass density  $\rho_{\text{gr}}$ . Then, the system response is a function of the following dimensionless parameters: stiffness of the fluid relative to the skeleton, defined through the ratio  $K_f/\mu_s$  and the Poisson’s ratio  $\nu_s$ ; mass density of the skeleton relative to the fluid, defined through the ratio  $\rho_{\text{gr}}/\rho_f$  and the porosity  $\hat{n}$ ; mass of the building relative to the mass of the foundation, and mass of the foundation relative to the mass of the replaced soil, through the ratios  $m_b/m_{\text{fnd}}$  and

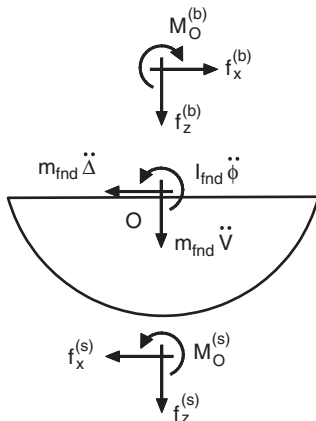


Fig. 3. Dynamic equilibrium of the foundation.

$m_{\text{find}}/m_{\text{gr}}$ , where,  $m_{\text{gr}} = A_{\text{find}}\rho_{\text{gr}}$  is the mass of the excavated soil (per unit length) if there were no voids, and  $A_{\text{find}}$  is the area of the foundation; the flexibility of the building relative to that of the soil, through the ratio  $\varepsilon = (V_{\text{ref}}H)/(V_{S,b}a) = [(\omega H)/V_{S,b}]/[(\omega a)/V_{\text{ref}}] =$  ratio of the number of wavelength in the shear beam in length  $H$  and the number of reference wavelengths in the soil in length  $a$ ; dimensionless frequency  $\eta = \omega a/(\pi V_{\text{ref}})$ , where  $V_{\text{ref}} = \sqrt{\mu_s/\rho_{\text{gr}}}$  is a reference velocity; foundation shape, through the ratio  $h/a$ ; and on the type, amplitude and angle of the incident waves.

The theoretical developments presented in this paper were implemented in the FORTRAN computer program SSI\_POROUS. In the companion paper [20], we will illustrate the results of this theoretical model, and will show results that correspond approximately to the conditions of Millikan Library. We will attempt to explain the observed increase of the system frequencies of Millikan library during heavy rainfall, and recovery of these frequencies within several days following the rainfall. The postulated hypothesis will be that the change in frequency is due to changes in the soil, in particular—increased foundation stiffness.

### Acknowledgements

We thank Prof. M. D. Trifunac for suggesting that we investigate this problem. He and Prof. V. W. Lee critically read the manuscript and offered may valuable suggestions.

### Appendix A

The terms of matrix  $[D(r)]_{2 \times 3}^{(l)}$  and  $[D(r)]_{2 \times 3}^{(f,j)}$  used to compute displacements of the skeleton and of the fluid in Eqs. (20a) and (20b) are

$$\begin{aligned} D_{11}^{(l)}(r) &= -nC_n(k_{P1}r) + k_{P1}rC_{n-1}(k_{P1}r), \\ D_{12}^{(l)}(r) &= -nC_n(k_{P2}r) + k_{P2}rC_{n-1}(k_{P2}r), \\ D_{13}^{(l\pm)}(r) &= \pm nC_n(k_{SR}), \\ D_{21}^{(l\pm)}(r) &= \mp nC_n(k_{P1}r), \\ D_{22}^{(l\pm)}(r) &= \mp nC_n(k_{P2}r), \\ D_{23}^{(l)}(r) &= nC_n(k_{SR}) - k_{\beta}rC_{n-1}(k_{SR}), \\ D_{ij}^{(f,j)}(r) &= f_j D_{ij}^{(l)}(r), \quad i = 1, 2; \quad j = 1, 2, 3, \end{aligned} \quad (\text{A.1a})$$

where

$$C_n(\cdot) = \begin{cases} J_n(\cdot), & l = 1, \\ Y_n(\cdot), & l = 2, \\ H_n^{(1)}(\cdot), & l = 3, \\ H_n^{(2)}(\cdot), & l = 4, \end{cases} \quad (\text{A.2})$$

$J_n(\cdot)$  and  $Y_n(\cdot)$  are the Bessel functions of first and second kind, and  $H_n^{(1)}(\cdot)$  and  $H_n^{(2)}(\cdot)$  are the Hankel functions of the first and second kind, and  $f_j$  is as defined in Eq. (10). Similarly, the terms of matrices  $[E(r)]_{2 \times 3}^{(l)}$  and  $[E(r)]_{1 \times 3}^{(f,j)}$  used to compute the stresses of the skeleton and of the fluid in Eq. (21a) and (21b) are

$$\begin{aligned} E_{11}^{(l)}(r) &= \left[ n^2 + n - \frac{1}{2}(k_{P1}r)^2 \right] C_n(k_{P1}r) \\ &\quad - \frac{1}{2}(k_{P1}r)^2 \left( 1 + \frac{\lambda}{2} + Q \right) C_n(k_{P1}r) \\ &\quad - k_{P1}rC_{n-1}(k_{P1}r), \\ E_{12}^{(l)}(r) &= \left[ n^2 + n - \frac{1}{2}(k_{P2}r)^2 \right] C_n(k_{P2}r) \\ &\quad - \frac{1}{2}(k_{P2}r)^2 \left( 1 + \frac{\lambda}{2} + Q \right) C_n(k_{P2}r) \\ &\quad - k_{P2}rC_{n-1}(k_{P2}r), \\ E_{13}^{(l\pm)}(r) &= \mp n[-(n+1)C_n(k_{SR}) + k_{SR}C_{n-1}(k_{\beta}r)], \\ E_{21}^{(l\pm)}(r) &= \mp n[-(n+1)C_n(k_{P1}r) + k_{P1}rC_{n-1}(k_{P1}r)], \\ E_{22}^{(l\pm)}(r) &= \mp n[-(n+1)C_n(k_{P2}r) + k_{P2}rC_{n-1}(k_{P2}r)], \\ E_{23}^{(l)}(r) &= - \left[ n^2 + n - \frac{1}{2}(k_{SR})^2 \right] C_n(k_{SR}) \\ &\quad - k_{SR}C_{n-1}(k_{SR}), \end{aligned} \quad (\text{A.3a})$$

$$\begin{aligned} E_{11}^{(f,j)}(r) &= \frac{1}{2} S_1(k_{P1}r)^2 C_n(k_{P1}r), \\ E_{12}^{(f,j)}(r) &= \frac{1}{2} S_2(k_{P2}r)^2 C_n(k_{P2}r), \\ E_{13}^{(f,j)}(r) &= 0, \end{aligned} \quad (\text{A.3b})$$

where

$$S_j = (Q + f_j R)/\mu, \quad j = 1, 2. \quad (\text{A.4})$$

### Appendix B

$$\begin{aligned} I_1(n) &= \int_{-\theta_0}^{\theta_0} \cos \theta_1 \cos n\theta_1 \, d\theta_1 \\ &= \begin{cases} \frac{\sin(n+1)\theta_0}{n+1} + \frac{\sin(n-1)\theta_0}{n-1}, & n \neq 1, \\ \frac{\sin 2\theta_0}{2} + \theta_0, & n = 1. \end{cases} \end{aligned} \quad (\text{B.1})$$

$$\begin{aligned} I_4(n) &= \int_{-\theta_0}^{\theta_0} \sin \theta_1 \sin n\theta_1 \, d\theta_1 \\ &= \begin{cases} \frac{-\sin(n+1)\theta_0}{n+1} + \frac{\sin(n-1)\theta_0}{n-1}, & n \neq 1, \\ \frac{-\sin 2\theta_0}{2} + \theta_0, & n = 1. \end{cases} \end{aligned} \quad (\text{B.2})$$

$$I_5(n) = \int_{-\theta_0}^{\theta_0} \cos n\theta_1 d\theta_1$$

$$= \begin{cases} \frac{2 \sin n\theta_0}{n}, & n \neq 1, \\ 2\theta_0, & n = 0. \end{cases} \quad (\text{B.3})$$

## References

- [1] Biot MA. General theory of three-dimensional consolidation. *J Appl Phys* 1941;12:155–64.
- [2] Biot MA. Theory of propagation of elastic waves in a fluid-saturated porous solid, I: low frequency range. *J Acoust Soc Am* 1956; 28:168–78.
- [3] Biot MA. Theory of propagation of elastic waves in a fluid-saturated porous solid, II: higher frequency range. *J Acoust Soc Am* 1956; 28:179–91.
- [4] Biot MA. Mechanics of deformation and acoustic propagation in porous media. *J Appl Phys* 1962;33:1482–98.
- [5] Halpern MR, Christiano P. Steady-state harmonic response of a rigid plate bearing on a liquid-saturated poroelastic half space. *Earthquake Eng Struct Dyn* 1986;14:439–54.
- [6] Philippacopoulos AJ. Axisymmetric vibration of disk resting on saturated layered half space. *J Eng Mech Div ASCE* 1989;115(10): 2301–22.
- [7] Bougacha S, Tassoulas JL, Roesset JM. Analysis of foundations on fluid-filled poroelastic stratum. *J Eng Mech ASCE* 1993;119(8): 1632–48.
- [8] Bougacha S, Roesset JM, Tassoulas JL. Dynamic stiffness of foundations on fluid filled poroelastic stratum. *J Eng Mech ASCE* 1993;119(8):1649–62.
- [9] Kassir MK, Xu JM. Interaction functions of a rigid strip bonded to saturated elastic half-space. *Int J Solids Struct* 1988;24(9):915–36.
- [10] Kassir MK, Bandyopadhyay KK, Xu J. Vertical vibration of a circular footing on a saturated half-space. *Int J Eng Sci* 1989; 27(4):353–61.
- [11] Rajapakse RKND, Senjuntichai T. Dynamic response of a multi-layered poroelastic medium. *Earthquake Eng Struct Dyn* 1995; 24:703–22.
- [12] Kassir MK, Xu J, Bandyopadhyay KK. Rotary and horizontal vibrations of a circular surface footing on a saturated elastic half-space. *Int J Solids Struct* 1996;33(2):265–81.
- [13] Dargush GF, Chopra MB. Dynamic analysis of axisymmetric foundations on poroelastic media. *J Eng Mech ASCE* 1996; 122(7):623–32.
- [14] Japon BR, Gallego R, Dominguez J. Dynamic stiffness of foundations on saturated poroelastic soils. *J Eng Mech ASCE* 1997; 123(11):1121–9.
- [15] Zeng X, Rajapakse RKND. Vertical vibrations of a rigid disk embedded in a poroelastic medium. *Int J Numer Analyt Meth Geomech* 1999;23:2075–95.
- [16] Bo J, Hua L. Vertical dynamic response of a disk on a saturated poroelastic half-space. *Soil Dyn Earthquake Eng* 1999;18:437–43.
- [17] Jin B, Liu H. Horizontal vibrations of a disk on a poroelastic half-space. *Soil Dyn Earthquake Eng* 2000;19:269–75.
- [18] Jin B, Liu H. Rocking vibrations of rigid disk on saturated poroelastic medium. *Soil Dyn Earthquake Eng* 2000;19:469–72.
- [19] Senjuntichai T, Mani S, Rajapakse RKND. Vertical vibration of an embedded rigid foundation in a poroelastic soil. *Soil Dyn Earthquake Eng* 2006, this issue, doi:10.1016/j.soildyn.2006.01.013.
- [20] Todorovska MI, Al Rjoub Y. Effects of rainfall on soil–structure system frequency: examples based on poroelasticity and a comparison with full-scale measurements. *Soil Dyn Earthquake Eng* 2006, this issue, doi:10.1016/j.soildyn.2006.01.019.
- [21] Popescu R, Prevost JH, Deodatis G, Chakraborty P. Dynamics of nonlinear porous media with applications to soil liquefaction. *Soil Dyn Earthquake Eng* 2006, this issue, doi:10.1016/j.soildyn.2006.01.015.
- [22] Luco JE. Dynamic interaction of a shear wall with the soil. *J Eng Mech ASCE* 1969;95:333–46.
- [23] Trifunac MD. Interaction of a shear wall with the soil for incident plane SH-waves. *Bull Seismological Soc Am* 1972;62:63–83.
- [24] Wong HL, Trifunac MD. Interaction of shear wall with the soil for incident plane SH waves: elliptical rigid foundation. *Bull Seismological Soc Am* 1974;64:1825–42.
- [25] Todorovska MI. Effects of the wave passage and the embedment depth during building-soil interaction. *Soil Dyn Earthquake Eng* 1993;12(6):343–55.
- [26] Todorovska MI. In-plane foundation-soil interaction for embedded circular foundations. *Soil Dyn Earthquake Eng* 1993;12(5):283–97.
- [27] Clinton JF, Bradford SK, Heaton TH, Favela J. The observed wander of the natural frequencies in a structure. *Bull Seismological Soc Am* 2006;96(1):237–57.
- [28] Lin C-H, Lee VW, Trifunac MD. On the reflection of elastic waves in a poroelastic half-space saturated with non-viscous fluid. Report CE 01-04, Department of Civil Engineering, University of Southern California.
- [29] Lin C-H, Lee VW, Trifunac MD. The reflection of plane waves in a poroelastic half-space saturated with inviscid fluid. *Soil Dyn Earthquake Eng* 2005;25:205–23.
- [30] Davis CA, Lee VW, Bardet JP. Transverse response of underground cavities and pipes to incident SV waves. *Earthquake Eng Struct Dyn* 2001;30(3):383–410.
- [31] Cao H, Lee VW. Scattering and diffraction of plane P waves by circular cylindrical canyons with variable depth-to-width ratio. *Soil Dyn Earthquake Eng* 1990;9(3):141–50.
- [32] de Barros FCP, Luco JE. Dynamic response of a two-dimensional semi-circular foundation embedded in a layered viscoelastic half-space. *Soil Dyn Earthquake Eng* 1995;14:45–57.
- [33] Deresiewicz H. The effects of boundaries on wave propagation in a liquid-filled porous solid: I. Reflection of plane waves at a free plane boundary (non-dissipative case). *Bull Seismological Soc Am* 1960; 50(4):599–607.
- [34] Biot MA, Willis DG. The elastic coefficients of a theory of consolidation. *J Appl Mech ASME* 1957;29:594–601.
- [35] Berryman JG. Confirmation of Biot's theory. *Appl Phys Lett* 1980;34(4):382–4.
- [36] Lee VW, Cao H. Diffraction of SV waves by circular cylindrical canyons of various depths. *A.S.C.E., Eng Mech Div* 1989;115(9): 2035–56.